(d), 18.8 (t), 18.0 (t), 17.4 (s), 15.7 (q), 15.6 (q); MS (relative intensity) m/z 222 (M^+, 24), 204 (100), 189 (99), 161 (50), 137 (54), 109 (83), 43 (74).

Preparation of the 2-Phenylbutanoyl Ester of Neomeranol. The 2-phenylbutyrate of neomeranol (**5**) was prepared from 8.4 mg of neomeranol and the acid chloride using procedures described recently.[13] The crude product was purified by HPLC (Ultrasphere-Cyano, 4:1 hexane-CH_2Cl_2) to give **7**, 3.8 mg: $[\alpha]_D$ -10.5° (c 0.38, $CHCl_3$); ^1H NMR ($CDCl_3$) δ 7.3-7.2 (5 H, br s), 4.64 (1 H, dd), 4.45 (1 H, dd), 3.45 (1 H, m), 2.28-2.20 (2 H, m), 1.91-1.50 (4 H, m), 1.35-1.10 (3 H, m), 1.08 (3 H, s), 0.98-0.95 (2 H, m), 0.91 (3 H, s), 0.89 (3 H, t), 0.78 (3 H, s), 0.70 (3 H, s), 0.56 (1 H, dd); MS (relative intensity) m/z 448 (M^+, 0.5), 367 (52), 282 (16), 203 (66), 119 (100), 95 (63). The optical rotation of the acid recovered from unreacted acid chloride was $[\alpha]_D$ -15.6° (c 0.45, $CHCl_3$), corresponding to an optical yield of 21%.[12]

Acknowledgment. We thank L. J. Sears for the accurate mass measurements and Professor T. Livinghouse for helpful suggestions. This work was supported by the Office of Sea Grant, Department of Commerce, the Montana Agricultural Experiment Station, and, in part, by Grant CA 35905 from the National Cancer Institute and Grant E-792 from the Robert A. Welch Foundation.

Revisiting Kaolinite Dehydroxylation: A ^{29}Si and ^{27}Al MAS NMR Study

J. F. Lambert, W. S. Millman, and J. J. Fripiat*

Contribution from the Laboratory for Surface Studies and Department of Chemistry, University of Wisconsin—Milwaukee, Milwaukee, Wisconsin 53201. *Received June 20, 1988*

Abstract: The ^{29}Si and ^{27}Al MAS NMR spectra of kaolinite are easily interpreted in terms of a Q^3 environment for silicon and of an octahedral configuration of aluminum. Upon progressive dehydroxylation, these spectra become more complex. For a degree of dehydroxylation (α) between 1/10 and 9/10, three ^{27}Al resonances are observed at +3, +28, and +55 ppm. The octahedral component decreases in intensity as α increases, whereas the other two become dominant. The line at +28 ppm is assigned to pentacoordinated Al, as suggested by Gilson et al. (*J. Chem. Soc., Chem. Commun.* **1987**, 91). The +55-ppm line is attributed to tetrahedrally coordinated Al. Simultaneously, the -91-ppm (initial) component of the ^{29}Si spectrum decreases in intensity, while at least two components corresponding to more shielded Si nuclei grow in intensity. As α increases beyond 9/10, further shifts are observed in the ^{29}Si spectra as mentioned by Meinhold et al. (*J. Mater. Sci. Lett.* **1985**, *4*, 163). Ultimately a line at -109 ppm suggests a significant proportion of the ^{29}Si nuclei being in a Q^4 environment, while the ^{27}Al spectrum is reminiscent of that of a spinel-like material. The relationships between the ^{29}Si and ^{27}Al spectra are discussed and compared with IR data in the 1200-400-cm^{-1} range and with earlier results on ^1H (static) NMR.

The mechanism by which kaolinite loses water has attracted much attention over the past century. The structure of the material has been well characterized, and numerous studies have been devoted to the kinetic process. The structural arrangement in the dehydration product, i.e., metakaolinite, was studied by several groups, the most classical work being that of Brindley and Nakahira.[1] They concluded that during the dehydration the original atomic ordering along the a and b axes was maintained, but that it disappeared along the c axis.[2] Accordingly, they showed that the coordination number of the aluminum changes from 6-fold to 4-fold and that the reaction proceeds by successive dehydroxylation of the octahedral layers. Indeed, the intensity of the [001] X-ray reflection shows an inverse linear decrease with the extent of dehydroxylation (α). Moreover, up to $\alpha = 0.6$, the second moment of the ^1H NMR resonance line is nearly constant.[3] If the dehydroxylation occurred by the growth of randomly distributed nuclei, the average proton-proton distance should increase with α and the second moment should decrease rapidly as predicted by its $1/r^6$ dependence. This behavior of the second moment was recently confirmed,[4] in a study of the proton resonance as a function of α, covering a range of $\alpha \approx 0$ to $\alpha = 0.97$. For $\alpha < 0.7$ the second moment was invariant. However, for $0.7 < \alpha \leq 0.97$, the remaining protons distribute themselves among two population of sites. This latter conclusion was reached by distinguishing between the proton-proton interaction and the proton-aluminum interaction using the Carr-Purcell pulse sequence to separate the heteronuclear dipolar coupling (plus shielding anisotropy) from the homonuclear dipolar broadening. In the range $\alpha > 0.7$, the proton-proton second moment decreases from 6 to 1 G^2, whereas the ^1H-^{27}Al second moment remains at about 1.4 G^2. The proton population with the decreasing ^1H-^1H moment was assumed to be within shrinking patches of Al(OH) octahedra. The second population was suggested to be composed of isolated protons interacting with aluminum.

Meinhold et al.[5] were among the first to study the high-temperature transformation of metakaolinite into mullite, which occurs above 900 °C, using high-resolution solid-state ^{27}Al and ^{29}Si NMR. In spite of relatively poor resolution (the field was 4.7 T and the spinning rate was 2.6 kHz), they observed a ^{27}Al resonance at 35 ppm in addition to those at 65 and 0 ppm for tetrahedrally and octahedrally coordinated aluminum, respectively. The resonance at 35 ppm was upfield of any previously reported resonance for tetrahedrally coordinated aluminosilicates. In conjunction with the transformations of the ^{27}Al spectra, the ^{29}Si spectra broadened and shifted from that observed in kaolinite (-91.5 ppm) to about -100 ppm. At temperatures above 900 °C, the ^{29}Si spectrum was found to consist of a resonance at about -110 ppm with a shoulder at about -88 ppm. The upfield shift was considered to reflect a decrease in the number of Al groups bonded to the SiO_4 tetrahedral units.

In studying metakaolinite at higher fields and spinning rates (9.4 T), Gilson et al.[6] went further in interpreting the ^{27}Al MAS

* To whom all correspondence should be addressed.

(1) Brindley, G. W.; Nakahira, M. *Mineral. Mag.* **1958**, *31*, 781.
(2) Brindley, G. W.; Nakahira, M. *J. Am. Ceram. Soc.* **1959**, *42*, 311.
(3) Gastuche, M. C.; Toussaint, F.; Touilleaux; Fripiat, J. J.; Van Meersch, M. *Clay Mineral. Bull.* **1963**, *5*, 227.
(4) Otero-Arean, C.; Letellier, M.; Gerstein, B. C.; Fripiat, J. J., *Proceedings of the International Clay Conference, 1981*; (Van Olphen and Veniale, Eds.; Elsevier, New York, 1982; p 73.
(5) Meinhold, R. H.; MacKenzie, K. J. D.; Brown, I. W. M. *J. Mater. Sci. Lett.* **1985**, *4*, 163.

0002-7863/89/1511-3517$01.50/0

NMR spectrum. They observed the same three peaks with the middle one at 31.2 ppm. They assigned this peak to pentacoordinated aluminum. Alemany et al.[7] reported, indeed, an isotropic chemical shift at +35 ppm for 5-fold coordinated aluminum in andalusite, where this species is in distorted trigonal bipyramids.[8] Moreover, Gilson et al.[6] did not publish silicon spectra which would have permitted comparison with the ^{27}Al resonance data.

The aim of the present contribution is to bridge the gap between these different studies by studying kaolinite at different degrees of dehydroxylation (α). This important information did not appear in a paper by Watanabe et al.,[9] who studied the transformation of kaolinite by MAS NMR of ^{29}Si and ^{27}Al at 7 T and between 3 and 4 kHz spinning rate. They did not eliminate the possibility of pentacoordinated aluminum being present, but were unable to detect its presence. This is likely to be due to a number of experimental problems such as the low spinning rate resulting in overlap of spinning side bands from both the tetrahedral and octahedral resonances and the effect of the low magnetic field on the second-order quadrupolar Hamiltonian on the line widths. The latter effect is apparent in the 22-ppm width of the octahedral Al line in their spectra at 7 T, whereas at 11.7 T, as shown in this work, the width is only about 10 ppm in the starting material.

Experimental Section

A Davison kaolin clay was used in this study. It is a well-crystallized kaolinite with chemical formula $Al_2O_3 \cdot 2SiO_2 \cdot 2H_2O$ containing 1.2 wt % Fe_2O_3, 1.6 wt % TiO_2, and quartz as chemical and mineralogical impurities. The material was used without further purification. Dehydroxylation was achieved by heating for 1 h at temperatures between 400 and 1000 °C at intervals of 50 °C. In this way 13 samples were obtained with α varying between 0 and 0.97, α = (observed weight loss/maximum weight loss). The observed weight loss was that obtained by further heating of a portion of each sample for 14 h at 950 °C. The maximum weight loss was that obtained on calcination of a fresh sample dehydrated at 120 °C, from 120 to 950 °C.

When α was 0, X-ray diffractograms showed reflections typical of a well-crystallized kaolinite with an additional weak reflection at 3.40 Å, due to the quartz impurity. The diffractograms were obtained on a Phillips goniometer using Ni-filtered Cu Kα radiation. Consistent with earlier work, the intensities of the 001 and 002 reflections weakened with increasing α and disappeared at α = 0.796. As α increased from 0.796 to 0.97, a broad background centered at 15° 2θ grew in intensity. Finally, at α = 0.96 a weak reflection appeared at about 45° 2θ. This latter reflection is consistent with the formation of the spinel phase which occurs at about 1000 °C. These changes in the X-ray patterns are classical and will not be commented on further. They are included to show the consistency in the material with previous literature. As expected the change in intensity of the 001 reflection with α is linear up to about α = 0.796.

IR Spectroscopy. Infrared spectra were recorded using a Nicolet MX-1 FT spectrometer equipped with a Nicolet 620 data station. Samples were prepared as 1% by weight in KBr. The pellets were outgassed at 200 °C for 1 h prior to obtaining spectra. Typically, the spectra obtained were the average of 100 acquisitions at 2 cm^{-1} resolution. The OH stretching region was used as a check of the dehydroxylation (Figure 1A). Its integrated intensity was found to vary linearly with α. The main region of interest in this study is that between 1300 and 400 cm^{-1}, which contains the lattice vibrations in addition to two Al–O–H bending modes at about 910 and 940 cm^{-1}.

NMR Spectroscopy. High-resolution magic angle spinning NMR studies were carried out on a General Electric GN-500 equipped with a "high-speed" Doty probe and high-power amplifiers. The ^{27}Al and ^{29}Si spectra were obtained at 130.3 and 99.3 MHz, respectively. The spinning rates used were between 7 and 10 kHz. The typical acquisition parameters used for the aluminum 1 pulse experiments were: pulse width, 0.45 μs; delay, 50 ms; number of acquisitions, 10 000; acquisition time, 25.6 ms. Typical line broadenings were 20 Hz for narrow-line and 100 Hz for the broad-line spectra; the andalusite ^{27}Al spectrum in Figure 3 is shown without line broadening. The rf power was adjusted so that the 90° pulse length of the ^{27}Al signal from the reference Al^{3+} solution was 4.2 μs. The typical parameters for silicon 1 pulse with proton decoupling were: pulse width, 7 μs; delay, 3 s; number of acquisitions, 15 000; acquisition time, 25.6 ms; and 70 W of rf power. As usual the chemical shifts for silicon were referenced to Me_4Si.

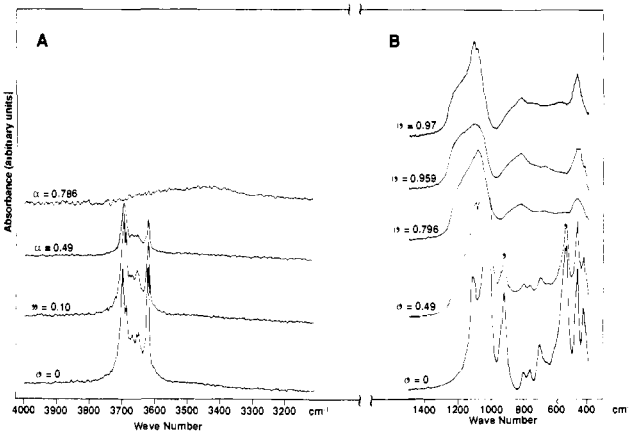

Figure 1. Typical FTIR spectra obtained at increasing α in (A) the 4000–3200-cm^{-1} range and (B) the 400–1500-cm^{-1} spectral domain.

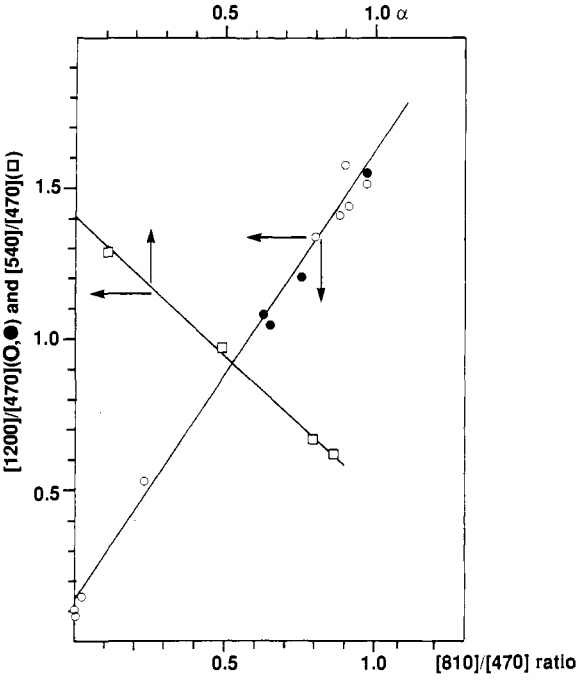

Figure 2. Variation of the 540 cm^{-1}/470 cm^{-1} absorbances ratio vs α (□) and variation of the 1200-cm^{-1}/470-cm^{-1} absorbances ratio vs the 810-cm^{-1}/470-cm^{-1} absorbances ratio; the open circles are obtained for $0 < \alpha < 0.95$, the dark circles for $\alpha > 0.95$.

Results

Infrared. The IR spectra in Figure 1 are shown as a function of α and are in agreement with the results of others. They are shown here to provide a basis for comparison of the vibrational bands from the tetrahedral and octahedral structural units with information obtained from MAS NMR. The onset of dehydroxylation results in a shoulder at about 1200 cm^{-1} on the low-frequency side of the Si–O out-of-plane stretch (1109 cm^{-1}). Also observed is an increase in the absorbance in the 810-cm^{-1} region along with a decrease in the 540–550-cm^{-1} region, which is characteristic of $Al–O_6$ octahedron stretching. As dehydroxylation proceeds, these trends become more evident. Since the tetrahedral deformation band near 470 cm^{-1} does not shift significantly throughout the dehydroxylation process, it can be used as a semiquantitative internal standard for comparison purposes.

The results of normalizing the changing bands at 1200, 810, and 540 cm^{-1} to the deformation band at 470 cm^{-1} are shown in

(6) Gilson, J. P.; Edwards, C.; Peters, A.; Koppuswamy, R.; Wormsbecher, R. F.; Roberie, T. G.; Shatlock, M. P. *J. Chem. Soc., Chem. Commun.* **1987**, 91.
(7) Alemany, L. B.; Kirker, G. W. *J. Am. Chem. Soc.* **1986**, *108*, 6158.
(8) Burnham, C. W.; Buerger, M. J., *Z. Kristallogr.* **1961**, *115*, 269.
(9) Watanabe, T.; Shimizu, H. J.; Nagasawa, K.; Masuda, A.; Saito, H. *Clay Mineral.* **1987**, *22*, 37.

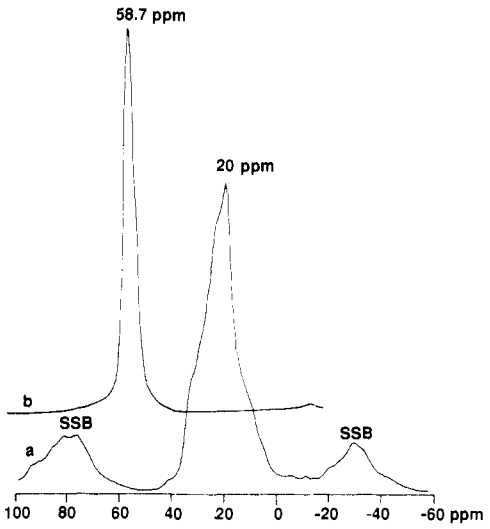

Figure 3. ^{27}Al MAS spectrum of (a) andalusite and (b) NaY-zeolite.

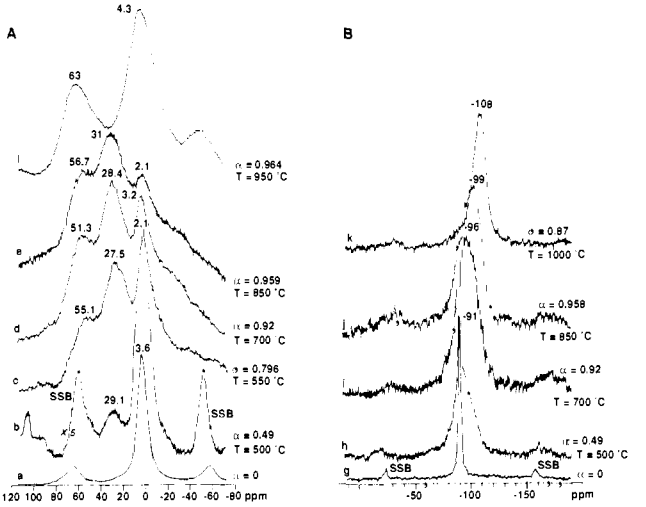

Figure 4. Selected ^{27}Al (A) and ^{29}Si spectra (B) observed at increasing α.

Figure 2. The 540-cm^{-1} band decreases and finally becomes unobservable in the region of $0.796 < \alpha < 0.847$. The 1200- and 810-cm^{-1} bands increase upon increasing α up until $\alpha = 0.95$. Beyond $\alpha = 0.95$, both decrease. The coupling of these two bands is demonstrated by the linear relationship between the intensity ratios 1200 cm^{-1}/470 cm^{-1} and 810 cm^{-1}/470 cm^{-1} in Figure 2. The band at 1025 cm^{-1}, in Figure 1, is replaced by a strong band at 1090 cm^{-1} as the extent of dehydroxylation reaches 0.84 and the latter persists up to $\alpha = 0.97$. It is clear that between $\alpha = 0.93$ and $\alpha = 0.96$ some rearrangement occurs. This is consistent with the results of Lemaitre et al.,[10] who suggested that a phase transition between metakalinite and mullite occurs between 800 and 900 °C.

NMR. Andalusite (spectrum a, Figure 3) is taken as reference for 5-fold coordinated Al (Al^V). The center of gravity (δ_{CG}) of the ($+^1/_2$,$-^1/_2$) central transition line shape is at 21.4 ppm with half-height width ($\nu_{1/2}$) of about 14 ppm, in excellent agreement with Alemany et al.[7] δ_{CG} is shifted from the true isotropic chemical shielding (δ_{CS}) by the second-order quadrupolar shift (δ_{QS}) (Lippmaa et al.[11]):

$$\delta_{CG} = \delta_{CS} + \delta_{QS} \quad (1)$$

where

$$\delta_{QS} = -6 \times 10^3 \frac{C_Q^2}{\omega_L^2}(1 + \eta^2/3) \text{ ppm} \quad (2)$$

for the central transition. The quadrupole coupling constant (C_Q) and asymmetry parameter η are 5.9 MHz and 0.69, respectively, in andalusite.[11] The Larmor frequency (ω_L) is 130.3 MHz. From eq 1 and 2 it follows that δ_{CS} is 35.6 ppm using the δ_{CG} observed here. This δ_{CS} is within +0.5 ppm of those reported in ref 11 and 7. If the line was Gaussian,[11] its width should be

$$\nu_{1/2} \text{ (ppm)} = (\ln 4)^{1/2}\delta_{QS} \quad (3)$$

or 16.5 ppm. The line is not Gaussian and it is slightly narrower than predicted by eq 3.

Spectrum b in Figure 3 represents the ^{27}Al resonance in NaY zeolite obtained under our acquisition conditions. The δ_{CG} of the Al^{IV} species is at 58.7 ppm, and $\nu_{1/2}$ is about 5 ppm. According to Samoson et al.,[12] the quadrupole coupling constant and asymmetry parameter of Al^{IV} in NaY are 2 MHz and $\eta = 0.5$, respectively. Using these parameters and eq 1 and 2 brings δ_{CS} to 60.5 ppm, as opposed to 62.8 ppm quoted in ref 11. $\nu_{1/2}$ should be 2 ppm if the line was Gaussian. This is much smaller than the experimental $\nu_{1/2}$ because line broadening factors other than the quadrupolar broadening are involved.

Spectrum a in Figure 4 is considered as typical for 6-fold coordinated Al (Al^{VI}). δ_{CG} is 3 ppm and $\nu_{1/2}$ is about 10 ppm. The main peak contains 74% of the total intensity of the ($^1/_2$, $-^1/_2$) transitions, the remaining 26% being shared by the first two spinning side bands (SSB), the other harmonics of the SSB being neglected. We shall consider the δ_{CS} shown above as characteristic for Al^{IV} and Al^V, whereas for Al^{VI} in kaolinite, we will admit that δ_{CG} and δ_{CS} coincide approximately. Note, however, that δ_{CS} for Al^V in barium aluminum glycolate and vesuvianite[13] are significantly higher.

The ^{29}Si spectra of the initial kaolinite (Figure 4g) has a resonance at −91.0 ppm from Me_4Si and a width at half-height of 2.5 ppm. This is in good agreement with Kinsey et al.[14] (−92 ppm, $\nu_{1/2}$ = 1.2 ppm) and Barron et al.[15] (−91 ppm, $\nu_{1/2}$ = 1.2 ppm) who obtained their spectra under cross-polarization conditions. This chemical shift is in the range of the Q^3 environment (Si−3Si) characteristic of layered silicates. It should be noted that the Q^4 resonance of the quartz impurity was not seen after 15 000 acquisitions under the recording conditions used here. At the onset of dehydroxylation there is no change in either the ^{27}Al or ^{29}Si spectrum. However, when α reaches 0.49, there is an increase in the background of the ^{27}Al spectrum near 20-30 ppm (Figure 4b) along with a broadening of the low-field spinning sideband (5 ppm) relative to the high-field spinning sideband, because of a contribution from an Al^{IV} resonance at 52 ppm. The ^{29}Si spectrum exhibits a shoulder at about −98 ppm (Figure 4h). Above 50% dehydroxylation, evidence for structural rearrangement of the silica tetrahedral network and a change in coordination number of Al^{VI} becomes stronger in the NMR spectra (Figure 4c, $\alpha = 0.796$).

When $\alpha \geq 0.796$ the ^{29}Si and ^{27}Al spectra are completely modified, Figure 4 d, i, and j. The width of the ^{29}Si resonance, which has its maximum near −98 ppm, increases to about 20 ppm, and the aluminum resonance now has three components at 3, 28, and ~55 ppm. For $\alpha = 0.92$, the peak at 28 ppm is the most intense. We shall tentatively assign these peaks to Al^{VI}, Al^V, and Al^{IV}, respectively. Qualitatively these features persist until $\alpha \leq 0.96$ (Figure 4, e and j). Quantitatively, as shown later, there are changes in the relative contributions of the components to these spectra, but overall, the spectra in Figure 4, c, d, and i, can be considered as representative of metakaolinite. The temperature range above 850 °C may be considered as that where phase

(10) Lemaitre, J.; Leonard, A. J.; Delmon, B. *Proceedings of the International Clay Conference, 1975*; Bailey, S. W., Ed. Applied Publishing; Ltd.: Wilmette, Ill., 1976; p 544.
(11) Lippmaa, E.; Samoson, A.; Mägi, M. *J. Am. Chem. Soc.* **1986**, *108*, 1730.
(12) Samoson, A.; Lippmaa, E. *Chem. Phys. Lett.* **1983**, *100*, 205.
(13) Phillips, B. L.; Allen, F. M.; Kirkpatrick, R. J. *Am. Miner.* **1987**, *72*, 1190.
(14) Kinsey, R. A.; Kirkpatrick, R. J.; Howes, J.; Smith, K. A.; Oldfield, E. *Am. Mineral.* **1985**, *70*, 537.
(15) Barron, P. F.; Frost, R. L.; Skjemstad, J. O.; Koppi, A. J. *Nature* **1983**, *302*, 49.

Table I. Deconvolution of the ^{29}Si Spectra into Gaussians[a]

sample no.	T (°C)	$\alpha/(1-\alpha)$	α	I: −91 ppm	−95 ppm	−98 ppm	−107 ± 3 ppm
85	350	0	0	100			
88	500	0.961	0.49	36.3		46.7	17
89	550	3.91	0.796	10.5		80	9.5
90	600	5.53	0.847	3		94.5	2.5
91	650	7.40	0.881	4.2		91.5	4.3
92	700	11.5	0.92	4.1		89.4	6.5
93	750	13.5	0.931	6.3		90.4	3.3
96	900	24.0	0.96		31.2		68.8
(94)	800	25.3	(0.962)	(15)	(2)	(79.8)	(4.2)
98	1000	31.3	0.97		13.1		86.9

[a] % total area; SSB excluded; I = relative intensity.

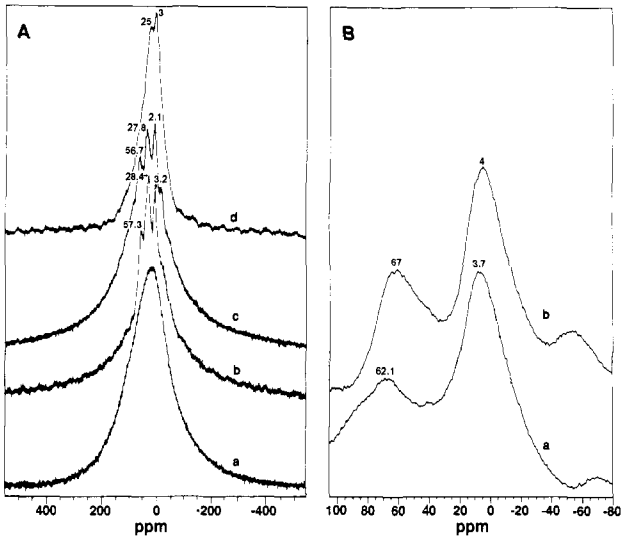

Figure 5. ^{27}Al resonance spectra of samples 92 (A) and 98 (B). (A) Wide scan spectra: (a) static, (b) spinning at 6.8 kHz, (c) spinning at 3.4 kHz, and (d) spectrum observed by shifting the frequency carrier to +55 ppm and by increasing the pulse length to 3.75 μs (see text). (B) 100, −80 ppm region: (a) spinning at 10 kHz, (b) spinning at 7.7 kHz.

segregation occurs (see Figure 4, f and k). ^{27}Al spectra as those displayed in Figures 5B and 4f are reminiscent of a transition (spinel-like) alumina. The ^{29}Si resonance line is at −107 ± 3 ppm, and it contains a contribution near ~−95 ppm (Figure 4k and Table I).

In order to understand the relationship between the appearance of both the penta- and tetracoordinated Al, an attempt to deconvolute both the ^{27}Al and the ^{29}Si spectra has been made. Deconvoluting the ^{27}Al spectra is not easy, as expected in view of the second-order quadrupolar shifts, line widths, and the overlap of various contributions. What follows should be considered as a *preliminary* attempt at the problem.

Let us consider wide scan static and MAS (spinning rates 3.4 and 6.8 kHz) ^{27}Al spectra shown in Figure 5A, spectra a, c, and b, respectively, as illustrations for metakaolinite. Spinning at 3.4 kHz does not reduce appreciably $\nu_{1/2}$, and spectrum c shows clearly three lines at 56.7, 27.8, and 2.1 ppm and two pairs of shoulders of similar intensity at 82 and −25 ppm and at 105 and −47.6 ppm, respectively. Spinning at 6.8 kHz leaves the three peaks (now at 57.3, 28.4, and 3.2 ppm) well resolved, but it narrows the low-field side of the signal. A larger magnification shows that the shoulders at 82 and 105 are still there. The upfield side of the signal is not affected. Thus, the two pairs of shoulders are not SSB. The unavoidable SSB should be 26 and 52 ppm apart from the main lines for spinning rates of 3.4 and 6.8 kHz, respectively. They must overlap with the main peaks and the shoulders.

Another experiment is shown in Figure 5d. This spectrum was obtained by shifting the frequency of the carrier in such a way that it coincides with the Al^{IV} line and the pulse length was

Table II. Main Features of the ^{27}Al MAS Resonance Spectra[a]

sample no.	T (°C)	α	$\alpha/(1-\alpha)$	Al^{IV} (ppm)	Al^{V} (ppm)	Al^{VI} (ppm)	I, %
85	350	0	0			3.6	100
88	500	0.49	0.961	(52)	(29.1)	3	<100
89	550	0.796	3.91	55.1	27.5	2.1	73
90	600	0.847	5.53	54	27	2	80
91	650	0.881	7.40	55	30	3	67
92	700	0.92	11.5	57	28	3	73
93	750	0.931	13.5	55	28.4	3	64
94[b]	800	0.962	25.3	54	29	3	65
95	850	0.959	23.4	57	31	2	72
96	900	0.96	24	59	30	4	72
97	950	0.964	26.8	65	(40.5)	4	65
98	1000	0.968	31.3	64	(40.4)	5	75

[a] I = contribution of the intensity between +120 and −80 ppm to the total intensity of wide scan ^{27}Al spectrum; T = dehydroxylation temperature; and α = degree of dehydroxylation. Average width, $\nu_{1/2}$; Al^{IV}, 3.4 kHz or 26 ppm; Al^{V}, 3.7 kHz or 28 ppm; Al^{VI}, 1.8 kHz or 14 ppm. [b] Anomalous value of α.

increased from 0.45 to 4.5 μs. With a pulse length of 3.75 μs, which was that used for spectrum d in Figure 5, there is a large decrease in intensity of the resonance at 55 ppm, and a general decrease in intensity of the down-field wing of the overall line shape. Under these conditions the line assigned to Al^{V} appears at 25 ppm, and it is still well differentiated from the Al^{VI} resonance at about 3 ppm. From this we conclude that there are indeed three Al sites.

Table II shows the position of these three peaks and the fraction of the total intensity contained in the 120, −80-ppm fraction of the overall spectrum. The average position of the Al^{IV} peak is at 55.3 ppm for the four samples 90–93 considered as representative of metakaolinite. The Al^{VI} peak is at 3 ppm. If we assume that δ_{CS} for Al^{IV} is 60 ppm, the C_Q for this species would be 3.8 MHz in metakaolinite if $\eta = 0$ (eq 1 and 2). The average position of the line assigned to Al^{V} for samples 89–95 is 28.7 ppm. With this value and assuming that δ_{CS} for Al^{V} is 35 ppm, C_Q for this species should be between 3.8 MHz ($\eta = 1$) and 4.4 MHz ($\eta = 0$).

Thus, C_Q's for Al^{IV} and Al^{V} are not dissimilar in metakaolinite. If the line with $\delta_{CG} = 28.7$ ppm were assigned to strongly distorted Al tetrahedra, its C_Q should be ≥9 MHz. Such a huge C_Q is not in the range reported by Lippmaa et al.[11] for tetrahedral sites. In steamed Y-zeolite where a line appears above 30 ppm, a 2D NMR investigation by Samoson et al.[16] indicates a quadrupole interaction exceeding 6 MHz for what they called "nonframework Al^{IV}". However, increasing the rf excitation pulse length from 0.5 μs up to 4.5 μs decreases selectively the intensity of this line, whereas it does not for metakaolinite (Figure 5d). These are the reasons for assigning the line observed in metakaolinite at +28.7 ppm to Al^{V}.

The variation in the quantitation of the contributions of the three peaks deals with a complicated situation, since C_Q for Al^{IV} *and* Al^{V} is on the order of 4 MHz, and overlapping side bands are beneath the three center bands. In such a situation, the best solution is probably the simplest. Therefore, we assume that we have in the 120, −80-ppm region a broad background from which three peaks emerge. Using 50% Gaussian and 50% Lorentzian peaks gave somewhat better fits than 100% Gaussian. We normalized the sum of the three contributions at 100% and expressed them in percent of residual intensity above the background. This procedure yields an average $\nu_{1/2}$ of 26 ppm for Al^{IV}, 28 ppm for Al^{V}, and 14 ppm for Al^{VI}. The relative intensities are displayed in Figure 6 with respect to $\alpha/(1-\alpha)$ and shift in ppm. By comparing different line shapes (from 0% Gaussian to 100% Gaussian) and repeated deconvolutions, the margin of uncertainty on the intensities is in the order of 10%. Before commenting on the results shown in Figure 6, let us examine the results of the ^{29}Si signal deconvolution.

(16) Samoson, A.; Lippmaa, E.; Engelhardt, G.; Lohse, U.; Jerschkewitz, H.-G. *Chem. Phys. Lett.* **1986**, *134*, 589.

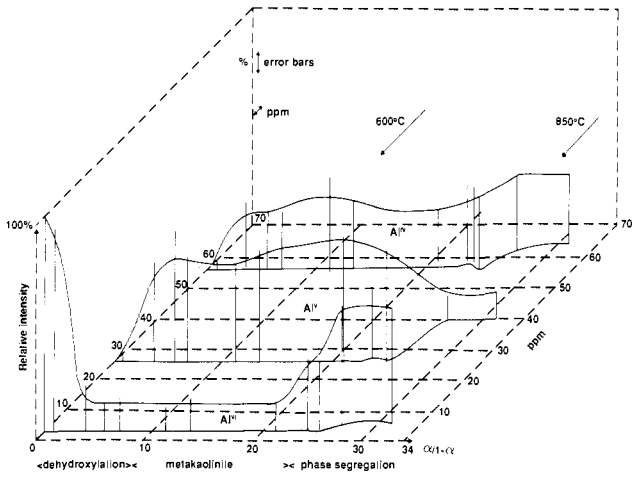

Figure 6. First-order approximation of the evolution of the Al^{VI}, Al^{V}, and Al^{IV} population (Table I) with respect to the fraction of reacted to unreacted material $\alpha/(1-\alpha)$ and the resonance frequency (ppm). The solid vertical lines are the relative intensities and the curves are the best fitting relative contents. Double-headed arrows show the average error bars for intensity and position of the lines.

Deconvolution of the ^{29}Si resonance is simpler because there is no interference from spinning side bands, the intensity of which can, to a first approximation, be neglected. The results of the deconvolution are shown in Table II. In the 300–600 °C range the Q^3 resonance at −91 ppm decreases in intensity with increasing α. Simultaneously, a resonance typical of a Q^4 environment appears. In Figure 4, spectra i and j, the resonance at −107 ± 3 ppm would be that of a Si with four Si next-nearest neighbors, whereas another at −98 ± 1 ppm would represent Si with an environment of 3 Si's and one Al neighbor. In the 650–750 °C range, $0.883 < \alpha < 0.931$, the Q^3 signal intensity at about −91 ppm is near zero while the intensity of the Q^4 lines represents 95% of the total signal. It is interesting to note that the intensity of the 1200- and 810-cm^{-1} vibrational bands increases nearly linearly with the total intensity of the Q^4 environment. In the temperature region where phase segregation occurs (800–900 °C), the relative abundance of the Q^4 environment (Si–3Si, 1Al) decreases. The results from sample 94 (see Tables I and II) are doubtful because of inconsistencies in the dehydroxylation temperature and the water content, especially with respect to sample 96. In samples 96 and 98 the ^{29}Si spectral fit required peaks at −109 and −95 ppm. That at −95 ppm could be due to a Q^4 environment with two Al neighbors.

On a *qualitative* basis there is a good agreement between the structural modifications shown by the evolution of the ^{29}Si and the ^{27}Al spectra. Between $\alpha = 0$ and $\alpha \simeq 0.847$ or $0 \leq \alpha/(1-\alpha) \leq 5.531$, there is a steep decrease in the intensity of the line assigned to Q^3 silicon and in the intensity of the Al^{VI} signal. Simultaneously, there is a fast increase in the intensity of the Al^{IV} and Al^{V} lines. It is all in the range of the dehydroxylation process (Figure 6). It is followed by a temperature domain where metakaolinite is metastable, $0.847 \leq \alpha \leq 0.96$ ($5.531 \leq \alpha/(1-\alpha) < 24$). The Q^3 silicon environment has practically disappeared and it is replaced by a Q^4 environment of (Si–4Si) and (Si–3Si, 1Al). In this range and within $\pm\simeq 10\%$, the *average* Al^{IV}, Al^{V}, and Al^{VI} contents are 32, 52, and 10%, respectively. The temperature domain of metakaolinite stability is between 600 and 850 °C. Above this temperature the Q^4 silicon environment is probably (Si–4Si) and (Si–2Si, 2Al). The Al^{V} line is replaced by a line at about 40 ppm with a low (10%) intensity and the Al^{VI} line becomes the dominant line. It broadens to ~40 ppm and shifts toward ~5 ppm. The Al^{IV} line intensity is larger than 30%. It contains, obviously, a contribution of the Al^{VI} line SSB as displayed in Figure 5B, where ^{27}Al spectra recorded with spinning rate 7.7 and 10 kHz are shown.

On a *quantitative* basis we have to examine whether or not the deconvolution procedure leading to Figure 6 makes any sense. Since the ^{29}Si deconvolution is much less open to criticism than the ^{27}Al deconvolution, let us calculate from the silicon spectrum the Al^{IV} content in metakaolinite. The Q^4 silicon signal contains (Si–4Si) and (Si–3Si, 1Al) contributions. Thus, the $(Si/Al)_{IV}$ content can be calculated from the

$$[I(-98\text{ ppm}) + I(-107\text{ ppm})]/[\tfrac{1}{4}I(-98\text{ ppm})] \quad (4)$$

intensity ratio. On the other hand, the chemical (Si/Al) ratio in kaolinite is 1. Thus, the inverse of the ratio calculated with eq 4, multiplied by 100, is the percent relative Al^{IV}/Al ratio. The average ratio obtained for the samples representative of metakaolinite is 24 ± 1.1%. This result has to be compared with the average Al^{IV} ratio obtained from the deconvolution of the Al spectra of the same samples, namely, 32 ± 6.1%, as reported above. The agreement is thus acceptable, and it may be concluded that the Al environment in metakaolinite can be approximated as follows: between 1/4 and 1/3 is in an Al^{IV} environment; ~1/2 is in an Al^{V} environment; and ~1/10 is in an Al^{VI} environment such as $Si\text{-}Al^{VI}$.

Discussion

It is clear that both the ^{27}Al and ^{29}Si high-resolution NMR results and the IR data cannot be interpreted by assuming that dehydroxylation and lattice reorganization occur in two consecutive steps. Indeed, for an $\alpha \simeq 0.49$, a Si Q^4 environment is already detectable and this implies the transformation of a bidimensional lattice into a tridimensional lattice. Moreover, everything happens in the region where the proton second moment is still almost constant. The Al^{VI} disproportionates into Al^{IV} and Al^{V}, and the Al^{IV} becomes part of a growing tridimensional lattice. It seems unlikely that pentacoordinated Al could be part of a tetrahedral lattice. It might be suggested that either it is the formation of Al^{V} which forces the bidimensional lattice to reorganize into a tridimensional lattice, or that it is the early (low α) reorganization which stabilizes Al^{V}.

The analysis of the ^{29}Si NMR results is supported by the evolution of the IR spectra and, in particular, by the relationship between the intensity of the 1200- and 810-cm^{-1} bands and the total Q^4 intensity $[I(-98\text{ ppm}) + I(-107\text{ ppm})]$. It has been shown earlier,[17] for silica gels, that the intensity of the 1200- and 810-cm^{-1} bands increases as the density of the gel decreases. Vibrational bands at about these frequencies are also reported by Flanigen[18] in steamed ultrastable Y-zeolite.

In the temperature domain where metakaolin is stable (second region in Figure 6), the material still contains between 12 and 4% of its initial water content. The initial silica network has disappeared as well as the hydroxylated octahedral aluminum. A new disordered tridimensional lattice is formed which contains silicon most likely linked to Al^{IV} and, in addition, pentacoordinated Al^{V}. It may be that the residual hydroxyls, whose second moment is $\approx 1.4\ G^2$ (ref 4), are actually bound to Al^{V}. However, it does not seem that there are enough OH left (in the region where $\alpha = 0.93 \pm 0.002$) to account for the high relative concentrations of Al^{V} shown in Figure 6.

In summary, the thermal transformations of kaolinite would occur in the three steps shown in Figure 6 over the temperature range between 400 and 1000 °C. Semiquantitatively, the comparison of the ^{29}Si and ^{27}Al resonances show reasonable agreement, and the three successive steps are supported by XRD, IR, and NMR.

Note should be taken that Lemaitre et al.[10] reported that the density of metakaolin decreases between 800 and 900 °C, i.e., at the onset of the segregation of a phase rich in alumina and of a phase rich in silica, according to the scheme:

$$\underset{\text{metakaolinite}}{Al_2O_3SiO_2} \rightarrow x\gamma Al_2O_3 + \underset{\text{mullite}}{y(3Al_2O_3{\cdot}2SiO_2)} + \underset{\text{amorphous}}{(1-x-3y)Al_2O_3{\cdot}(2-2y)SiO_2}$$

(17) Fripiat, J. J.; Leonard, A. J.; Barake, N. *Bull. Soc. Chim. Fr.* **1963**, 122.

(18) Flanigen, E. Zeolite Chemistry and Catalysis. *ACS Symp. Ser.* **1976**, *No. 171*, 106.

If we compare their suggestion with the data in Figure 6, we indeed observe, for $\alpha > 0.93$, the reappearance of a new form of Al^{VI} and the disappearance of Al^{V} (for $\alpha > 0.96$ or $\alpha/(1-\alpha) \geq 24$). Finally, above 900 °C, the ^{29}Si and ^{27}Al spectra are consistent with existence of γ-alumina mixed with ill-defined alumino-silicates, in agreement with Meinhold et al.[5] In the alumino-silicate phase, there would be silicon with two Al^{IV} neighbors (samples 96 and 98, Table II).

In conclusion, this work constitutes an additional proof of the capability of high-resolution solid-state NMR for solving problems related to disordered materials.

Acknowledgment. One of us (J.F.L.) thanks the Graduate School and the Laboratory for Surface Studies at UWM for a postdoctoral fellowship. The authors also wish to thank Dr. J. P. Gilson for drawing their attention to the problem treated in this paper and also for providing the samples. NSF Grant DIR-8719808 and NIH Grant RR 04095, which have partially supported the purchase of the GE500 NMR instrument, are gratefully acknowledged.

Ammonia Binds to the Catalytic Mn of the Oxygen-Evolving Complex of Photosystem II: Evidence by Electron Spin-Echo Envelope Modulation Spectroscopy†

R. David Britt,* Jean-Luc Zimmermann,‡ Kenneth Sauer, and Melvin P. Klein

Contribution from the Laboratory of Chemical Biodynamics, Lawrence Berkeley Laboratory, Berkeley, California 94720. *Received October 4, 1988*

Abstract: The mechanism of ammonia inhibition of photosynthetic oxygen evolution has been examined by the pulsed EPR technique of electron spin-echo envelope modulation (ESEEM), revealing the direct coordination of an ammonia-derived ligand to the catalytic Mn complex during the $S_1 \rightarrow S_2$ transition of the oxygen evolution S-state cycle. ESEEM experiments were performed on the "multiline" Mn EPR signal observed in photosystem II enriched spinach thylakoid membranes which were treated with either $^{14}NH_4Cl$ or $^{15}NH_4Cl$ (100 mM, pH 7.5). $^{15}NH_4Cl$ treatment produced modulation of the electron spin-echo signal which arises from an $I = {}^1/_2$ ^{15}N nucleus with an isotropic hyperfine coupling $A(^{15}N) = 3.22$ MHz. $^{14}NH_4Cl$ treatment produced a different ESEEM pattern resulting from an $I = 1$ ^{14}N nucleus with $A(^{14}N) = 2.29$ MHz, and with electric quadrupole parameters $e^2qQ = 1.61$ MHz and $\eta = 0.59$. The ^{14}N electric quadrupole parameters are interpreted with respect to possible chemical structures for the ligand. An amido (NH_2) bridge between metal ions is proposed as the molecular identity of the ammonia-derived ligand to the catalytic Mn of photosystem II.

Photosynthesis is the process by which plants and certain bacterial species convert photon energy into chemical energy. The resultant chemical energy is used to drive biochemical reactions. Higher plant photosynthesis involves two segregated photosystems. Photosystem I (PSI) acts to reduce water-soluble ferredoxin, and photosystem II (PSII) oxidizes water and produces O_2. The initial light-driven electron transfer event in photosystem II creates an electron-deficient pigment molecule with sufficient potential to perform water oxidation. The PSII water oxidation/oxygen evolution process is cyclic, with intermediate states of the oxygen-evolving complex (OEC) designated S_0 through S_4.[1] Each photooxidation of the primary pigment induces a transition in this S-state cycle. Molecular oxygen is released after four photooxidation events, and the complex resets to the least oxidized state, S_0. Each PSII reaction center contains four Mn atoms.[2] These form a protein-bound Mn complex that is thought to be the catalytic center for oxygen evolution. The structure of this Mn complex has been partially characterized by X-ray spectroscopy[3,4] and EPR.[5-12] Of particular interest is the discovery of a low-temperature "multiline" EPR signal which presents approximately 19 partially resolved hyperfine lines and is associated with the S_2 state of the Kok cycle.[5] The S_2 multiline EPR spectrum is rather similar to EPR spectra observed with di-μ-oxo bridged Mn(III)Mn(IV) dimers,[13] which suggests that the S_2 signal arises from a similar Mn complex. In such a model complex, the electronic spins of the two Mn ions are correlated by strong antiferromagnetic exchange interactions. The ground state has an effective electronic spin $\tilde{S} = {}^1/_2$. The EPR signal resulting from this effective spin is nearly isotropic and centered near $g = 2$. The EPR spectrum is split into 16 well-resolved lines resulting from hyperfine coupling to the two nonequivalent $I = {}^5/_2$ Mn nuclei. The PSII Mn multiline EPR signal results from an analogous exchange-coupled Mn complex, with hyperfine lines resulting from two or more Mn nuclei. Another S_2 EPR signal centered at the $g = 4.1$ region of the spectrum has also been assigned to paramagnetic Mn.[7,8,11,12,14] Analysis of details of EPR

† This is paper 10 in the series The State of Manganese in the Photosynthetic Apparatus.

‡ Present address: Service de Biophysique, Département de Biologie, Centre d'Etudes Nucléaires de Saclay, 91191 Gif-sur-Yvette Cedex, France.

(1) Kok, B.; Forbush, B.; McGloin, M. *Photochem. Photobiol.* **1970**, *11*, 457-475.
(2) Yocum, C. F.; Yerkes, C. T.; Blankenship, R. E.; Sharp, R. R.; Babcock, G. T. *Proc. Natl. Acad. Sci. U.S.A.* **1981**, *78*, 7507-7511.
(3) Yachandra, V. K.; Guiles, R. D.; McDermott, A.; Britt, R. D.; Dexheimer, S. L.; Sauer, K.; Klein, M. P. *Biochim. Biophys. Acta.* **1986**, *850*, 324-332.
(4) Yachandra, V. K.; Guiles, R. D.; McDermott, A. E.; Cole, J. L.; Britt, R. D.; Dexheimer, S. L.; Sauer, K.; Klein, M. P. *Biochemistry* **1987**, *26*, 5974-5981.
(5) Dismukes, G. C.; Siderer, Y. *Proc. Natl. Acad. Sci. U.S.A.* **1981**, *78*, 274-278.
(6) Hansson, Ö.; Andréasson, L.-E. *Biochim. Biophys. Acta* **1982**, *679*, 261-268.
(7) Casey, J. L.; Sauer, K. *Biochim. Biophys. Acta* **1984**, *767*, 21-28.
(8) Zimmermann, J. L.; Rutherford, A. W. *Biochim. Biophys. Acta* **1984**, *767*, 160-167.
(9) de Paula, J. C.; Brudvig, G. W. *J. Am. Chem. Soc.* **1985**, *107*, 2643-2648.
(10) de Paula, J. C.; Beck, W. F.; Brudvig, G. W. *J. Am. Chem. Soc.* **1986**, *108*, 4002-4009.
(11) Zimmermann, J. L.; Rutherford, A. W. *Biochemistry* **1986**, *25*, 4609-4615.
(12) Hansson, Ö.; Aasa, R.; Vänngård, T. *Biophys. J.* **1987**, *51*, 825-832.
(13) Cooper, S. R.; Dismukes, G. C.; Klein, M. P.; Calvin, M. *J. Am. Chem. Soc.* **1978**, *100*, 7248-7252.

0002-7863/89/1511-3522$01.50/0